Dynamics of Three-Dimensional Turbulent Wall Plumes and Implications for Estimates of Submarine Glacier Melting

EKATERINA EZHOVA

Institute for Atmospheric and Earth System Research, and Department of Physics, Faculty of Science, University of Helsinki, Helsinki, Finland

CLAUDIA CENEDESE

Physical Oceanography Department, Woods Hole Oceanographic Institution, Woods Hole, Massachusetts

LUCA BRANDT

Linné FLOW Centre, and Swedish e-Science Research Centre, Department of Mechanics, Royal Institute of Technology, Stockholm, Sweden

(Manuscript received 20 September 2017, in final form 29 June 2018)

ABSTRACT

Subglacial discharges have been observed to generate buoyant plumes along the ice face of Greenland tidewater glaciers. These plumes have been traditionally modeled using classical plume theory, and their characteristic parameters (e.g., velocity) are employed in the widely used three-equation melt parameterization. However, the applicability of plume theory for three-dimensional turbulent wall plumes is questionable because of the complex near-wall plume dynamics. In this study, corrections to the classical plume theory are introduced to account for the presence of a wall. In particular, the drag and entrainment coefficients are quantified for a three-dimensional turbulent wall plume using data from direct numerical simulations. The drag coefficient is found to be an order of magnitude larger than that for a boundary layer flow over a flat plate at a similar Reynolds number. This result suggests a significant increase in the melting estimates by the current parameterization. However, the volume flux in a wall plume is found to be one-half that of a conical plume that has 2 times the buoyancy flux. This finding suggests that the total entrainment (per unit area) of ambient water is the same and that the plume scalar characteristics (i.e., temperature and salinity) can be predicted reasonably well using classical plume theory.

1. Introduction

Subglacial discharge is among the major factors controlling submarine melting of Greenland's tidewater glaciers (Straneo and Cenedese 2015). Turbulent plumes generated by freshwater at the freezing temperature discharged at the glacier base enhance melting of the ice face. In Greenland the ice tongue has broken off in most tidewater glaciers and the ice face is quasi vertical; therefore, subglacial discharge plumes are usually modeled as a turbulent buoyant plume propagating along a vertical ice face (Straneo and Cenedese 2015).

Current ice–ocean models quantify melting employing the three-equation formulation by Holland and Jenkins (1999), where the effect of plume turbulence is parameterized through the friction velocity u_*, which is a fundamental parameter defining wall-bounded turbulence, and the melting rate is assumed to be proportional to u_*. To estimate the friction velocity from the mean velocity profile, a drag coefficient is typically used:

$$C_d = \frac{\tau}{\rho U_{\text{ref}}^2} = \frac{u_*^2}{U_{\text{ref}}^2}, \tag{1}$$

where $\tau = \rho\langle u_i' u_j' \rangle$ is the mean turbulent stress parallel to the ice face, U_{ref} is the reference velocity, and ρ is the water density. The drag coefficient is usually taken to be of order $C_d \approx 0.001$, a value close to that of a turbulent boundary layer flow over a flat plate at high Reynolds numbers (e.g., Monin et al. 1971). However, a

Supplemental information related to this paper is available at the Journals Online website: https://doi.org/10.1175/JPO-D-17-0194.s1.

Corresponding author: Ekaterina Ezhova, ekaterina.ezhova@helsinki.fi

DOI: 10.1175/JPO-D-17-0194.1

three-dimensional wall plume can be expected to exhibit strong lateral spreading similar to what was reported for the more extensively investigated wall jets (Launder and Rodi 1983). This effect is attributed by these authors to the secondary flows in the jet as well as to the gradients of turbulent stresses, the latter being more important (Craft and Launder 2001). An assumption that the turbulent stresses are similar to those in the two-dimensional boundary layer flow over a flat plate is thus not justified. A recent study (Slater et al. 2016) used a larger value of $C_d = 0.01$ following Jenkins et al. (2010), who found that this larger value of C_d was necessary to predict the observed melt rates of an ice shelf in Antarctica. In addition, current estimates of entrainment in wall plumes are based on experimental data and theoretical models for conical free plumes (Cowton et al. 2015; Slater et al. 2016; Mankoff et al. 2016).

The main focus of this study is to compare the modification of the classical plume theory for a three-dimensional turbulent wall plume with direct numerical simulations (DNS) and to quantify the drag and entrainment coefficients consistent with the theory using data from DNS and existing experiments. An appropriate drag coefficient is obtained by applying the modified plume theory to our simulations, and for this we use an analytical solution that, to our knowledge, is novel for 3D flows [2D analogs are reported by Gayen et al. (2016)]. As a first step, we consider a turbulent plume along a vertical wall without the meltwater feedback; that is, we assume that the wall is neither a source of mass nor a source of buoyancy.

2. Wall plume theory

Following Cowton et al. (2015), we consider the wall plume as one-half of a conical plume and assume that it can be described by the classical system of equations suggested by Morton et al. (1956) (this approach will be justified later by means of DNS). This theory is referred hereinafter as a modified Morton–Taylor–Turner (MTT) theory: the conservation equations for volume $\tilde{Q}$, momentum $\tilde{M}$, and buoyancy $\tilde{F}$ fluxes are written, following Cowton et al. (2015) and Slater et al. (2016), as

$$\frac{d\tilde{Q}}{d\tilde{z}} = \frac{d}{d\tilde{z}}(\pi\tilde{b}^2\tilde{u}/2) = \pi\alpha\tilde{b}\tilde{u}, \tag{2}$$

$$\frac{d\tilde{M}}{d\tilde{z}} = \frac{d}{d\tilde{z}}(\pi\tilde{b}^2\tilde{u}^2/2) = \pi\tilde{b}^2 g'/2 - 2C_d\tilde{b}\tilde{u}^2, \quad \text{and} \tag{3}$$

$$\frac{d\tilde{F}}{d\tilde{z}} = \frac{d}{d\tilde{z}}(\pi\tilde{b}^2\tilde{u}g'/2) = 0. \tag{4}$$

In the above, $\tilde{b}$ is the dimensional plume radius, $\tilde{u}$ is the dimensional plume velocity (assuming a top-hat velocity profile), $g' = g\Delta\tilde{\rho}/\tilde{\rho}_0$ is the reduced gravity, C_d is the drag coefficient, and α is the entrainment coefficient. The latter is defined as $\tilde{u}_e = \alpha\tilde{u}$, where $\tilde{u}_e$ is the entrainment velocity. Note that, because of the presence of a wall, α is not necessarily equal to that for a conical plume. Moreover, to account for a possible asymmetry in the plume shape, we introduce an "equivalent" radius $\tilde{b}$ (to be defined in terms of momentum and volume fluxes).

The system comprising Eqs. (2)–(4) is nondimensionalized by introducing the following variables: $Q = \tilde{Q}/(\tilde{b}_0^2\tilde{u}_0)$, $M = \tilde{M}/(\tilde{b}_0^2\tilde{u}_0^2)$, $F = \tilde{F}\mathrm{Fr}_0^2/(\tilde{b}_0\tilde{u}_0^3)$, and $z = \tilde{z}/\tilde{b}_0$, where $\mathrm{Fr}_0 = \tilde{u}_0/\sqrt{g_0'\tilde{b}_0}$ is the source Froude number and the subscript 0 indicates values at the source. Equations (2) and (3) can be rewritten as

$$dQ/dz = \sqrt{2\pi}\alpha M^{1/2} \quad \text{and} \tag{5}$$

$$\frac{dM}{dz} = \frac{F_0 Q}{\mathrm{Fr}_0^2 M} - \sqrt{8/\pi}C_d M^{3/2}Q^{-1}. \tag{6}$$

When neglecting the effect of a wall on the plume dynamics (hereinafter called a "free" plume), the drag term in Eq. (6) is assumed to be zero and

$$\frac{dM}{dQ} = \frac{F_0 Q}{\sqrt{2\pi}\alpha\mathrm{Fr}_0^2 M^{3/2}}, \tag{7}$$

which has the following analytical solution:

$$M^{5/2} = M_0^{5/2} + \frac{5F_0(Q^2 - Q_0^2)}{4\sqrt{2\pi}\alpha\mathrm{Fr}_0^2}. \tag{8}$$

However, in the presence of a wall, the drag term in Eq. (6) should be considered, which leads to

$$\frac{dM}{dQ} = \frac{F_0 Q}{\sqrt{2\pi}\alpha_w\mathrm{Fr}_0^2 M^{3/2}} - \frac{2}{\pi\alpha_w}C_d\frac{M}{Q}. \tag{9}$$

The solution therefore becomes (see the online supplementary material for the details of the derivation)

$$M^{5/2} = \frac{5F_0Q^2}{4\sqrt{2\pi}\alpha_w\mathrm{Fr}_0^2\left(1 + \dfrac{5C_d}{2\pi\alpha_w}\right)} + \left[M_0^{5/2} - \frac{5F_0Q_0^2}{4\sqrt{2\pi}\alpha_w\mathrm{Fr}_0^2\left(1 + \dfrac{5C_D}{2\pi\alpha_w}\right)}\right]\left(\frac{Q_0}{Q}\right)^{\frac{5C_d}{\pi\alpha_w}}, \tag{10}$$

where α_w is the entrainment coefficient in the presence of a wall.

The first term on the rhs of Eq. (10) grows with Q whereas the second term decreases; therefore, for $Q \gg Q_0$,

that is, sufficiently far from the source, the second term on the rhs of Eq. (10) can be neglected. Therefore, in the far field (i.e., for $M \gg M_0$ and $Q \gg Q_0$), the ratio $M^{5/2}/Q^2$ is constant for both the free [Eq. (8)] and wall [Eq. (10)] plume, and the drag and turbulent entrainment coefficients define the difference between these two cases. Since C_d is taken to be small in current models (Cowton et al. 2015; Slater et al. 2016), the wall plume is assumed to behave as a half-conical free plume. This, however, should be treated with caution. We show in what follows that the drag coefficient is an order of magnitude larger than can be expected when compared with the boundary layer flow over a flat plate.

The entrainment coefficient for a free plume can be obtained from the MTT theory [$b = (6/5)\alpha z$] if one knows the evolution of the plume radius with the distance from the source. The far-field asymptotic solutions for the wall plume radius and velocity can be obtained substituting the first term on the rhs of Eq. (10) in Eq. (5) and combining the solution with the definitions of the volume and momentum fluxes:

$$b_w = (6/5)\alpha_w z \quad \text{and} \tag{11}$$

$$u_w = \left(\frac{\alpha}{\alpha_w}\right)^{2/3} \frac{u}{\left(1 + \dfrac{5C_d}{2\pi\alpha_w}\right)^{1/3}}, \tag{12}$$

where

$$u = \left(\frac{5F_0}{4\pi\alpha \mathrm{Fr}_0^2}\right)^{1/3} \left(\frac{6\alpha z}{5}\right)^{-1/3}$$

is the classical MTT self-similar solution for a conical plume in a homogeneous fluid and the subscript w indicates wall plume properties.

In what follows, we quantify the entrainment and drag coefficients using data from DNS. In particular, we use the radius dependence on the distance from the source to define the entrainment coefficients for free and wall plumes and then quantify the drag coefficient based on the far-field solutions of Eqs. (8) and (10).

3. Results

Two simulations of a turbulent vertical lazy plume in a homogeneous fluid were performed: one conical plume and one wall plume. The conical plume is generated by a source volume flux $2\tilde{Q}_0$ exiting from a round source of radius $\tilde{b}_0$. The source Froude number of the plume is $\mathrm{Fr}_0 = \tilde{u}_0/(g_0'\tilde{b}_0)^{1/2} = 0.66$ and the Reynolds number $\mathrm{Re}_0 = \tilde{u}_0\tilde{b}_0/\nu = 1000$, where ν is the kinematic viscosity. The Froude number chosen here corresponds to that of a lazy plume, typical of those generated by a subglacial discharge. Note that a lazy plume gains velocity near the source because of its buoyancy (e.g., Fischer et al. 1979); for the Froude number used here the equivalent top-hat velocity near the source becomes approximately 2 times the source velocity, and, consequently, the effective Reynolds number near the source also increases by nearly a factor of 2. The wall plume is generated from a half-round source of radius $\tilde{b}_0$ attached to a wall with a total discharge $\tilde{Q}_0$ (see visualization in Fig. 1, left panel).

The DNS has been performed using the Nek5000 spectral-element code (Argonne National Laboratory; https://nek5000.mcs.anl.gov/). We consider an incompressible fluid with buoyancy modeled by the Boussinesq approximation. A cylindrical domain is used to simulate the conical plume, whereas a half cylinder is used for the wall plume, with an increased resolution close to the wall. The domain radius is $10\tilde{b}_0$, and the vertical length is $29\tilde{b}_0$. The resolution is less than $0.01\tilde{b}_0$ near the wall [or, in terms of inner scaling, $\Delta x \le 0.8x_\nu$, where $x_\nu = (\mathrm{Re}_0 u_*)^{-1}$ is the viscous length scale, except in a small domain in the vicinity of the symmetry axis where the resolution is $\Delta x \approx x_\nu$] and is close to $0.01\tilde{b}_0$ in the plume; therefore, we resolve the viscous sublayer as well as the plume up to the Kolmogorov scale of this flow, estimated as $\tilde{b}_0/\mathrm{Re}^{3/4} \approx 0.01\tilde{b}_0$. The total number of nodes is about 29 million for the wall plume and 46 million for the conical plume. We use the open (zero gradient) boundary conditions for the vertical velocity and density, combined with a sponge layer for the density fluctuations and horizontal velocity at the top outflow boundary, open boundary conditions for all variables, and a sponge layer for the density fluctuations on the open domain sides (cf. Ezhova et al. 2017). We set zero velocity and zero buoyancy flux at the wall.

a. *Comparison between wall plume theory and DNS results: Estimates of drag and entrainment coefficients using the wall plume theory*

The DNS results show that a wall plume indeed behaves similarly to a wall jet, being wider in the direction parallel to the wall and narrower perpendicular to the wall, as illustrated by Fig. 1 (top- and bottom-right panels).

The volume and momentum fluxes are computed at horizontal cross sections at each vertical z level as $Q = \iint U\,dx\,dy$ and $M = \iint U^2\,dx\,dy$. The nondimensional mean vertical velocity U is an average over 50 nondimensional time units (the eddy turnover time near

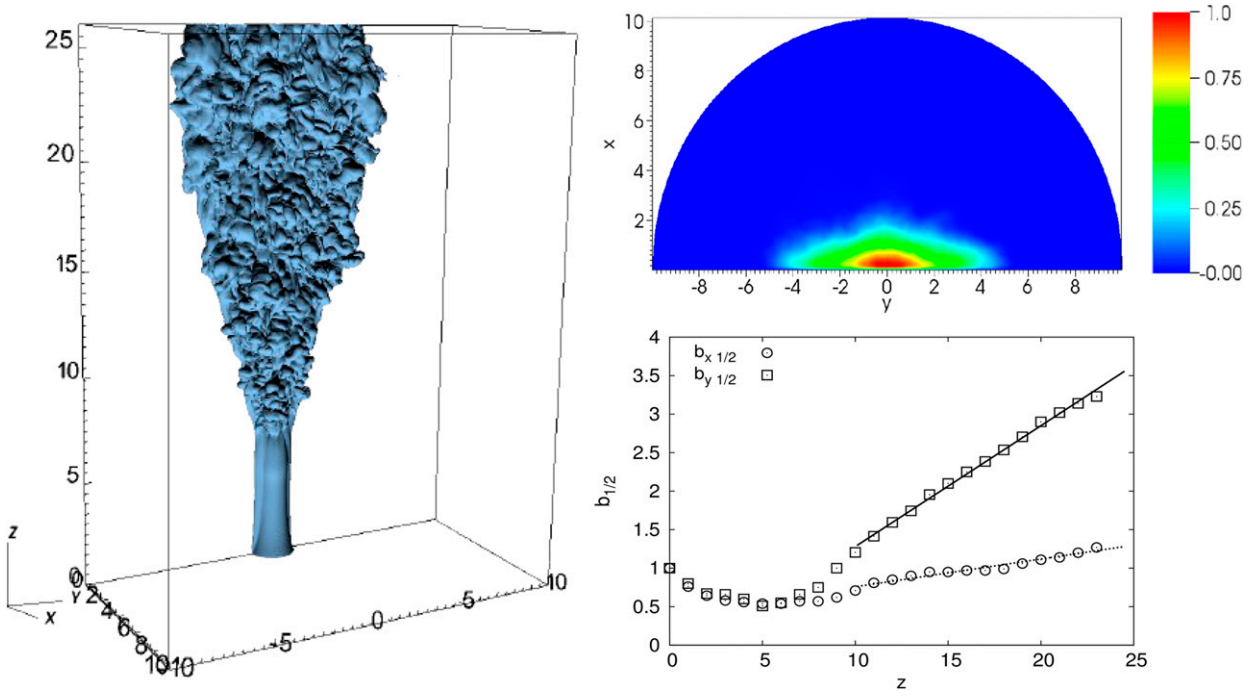

FIG. 1. (left) Wall plume visualized by the density contour $\rho = (\tilde{\rho} - \tilde{\rho}_{\rm pl})/(\tilde{\rho}_{\rm amb} - \tilde{\rho}_{\rm pl}) = 0.99$, where $\tilde{\rho}_{\rm pl}$ is the plume density and $\tilde{\rho}_{\rm amb}$ is the density of the ambient fluid. (top right) Mean vertical velocity at the cross-section $z = 20$ normalized with the maximum velocity in this cross section. (bottom right) Characteristic radii of the wall plume $b_{1/2}$ in the x and y directions vs vertical coordinate z; $b_{1/2}$ is defined as the radius at which the mean maximum velocity is halved. Best fits of the data for $z \geq 10$ have the slopes $s_x = 0.036$ and $s_y = 0.157$.

the top boundary is approximately 2 time units for the wall plume and 1.7 for the conical plume, where time is nondimensionalized using $t = \tilde{b}_0/\tilde{u}_0$). The values for a half-conical free plume are obtained by dividing by 2 the values from a conical plume.

The volume flux of the wall plume is almost identical to half of the volume flux pertaining the conical plume, whereas away from the source the momentum flux of the wall plume is reduced by approximately 15% when compared with that of the free plume as a result of the wall friction (Fig. 2). A similar result, that is, same volume fluxes and significant reduction of momentum flux in the presence of a wall, has been reported for three-dimensional turbulent wall jets by Namgyal and Hall (2016). In agreement with the modified MTT theory solutions for wall plumes (dashed lines in Fig. 2), the volume and momentum fluxes increase with distance from the source as $Q \sim z^{5/3}$ and $M \sim z^{4/3}$ (see the online supplementary material for a detailed derivation).

The equivalent plume radius is calculated at each vertical z level as $b = [(2Q^2)/(\pi M)]^{1/2}$, and, using the relationship $b = (6/5)\alpha z$, we determine the entrainment coefficient α for the two cases considered (Fig. 3). The entrainment coefficient pertaining to the wall plume is slightly larger than that for the conical plume: $\alpha_w = 0.110$ and $\alpha = 0.102$, respectively. Using the entrainment coefficients, we therefore proceed with the estimate of the drag coefficient by means of Eqs. (8) and (10). As discussed above, we neglect the second term on the rhs of Eq. (10) and use the far-field formulations of Eqs. (8) and (10) to obtain the ratio $M^{5/2}/Q^2$ for both free and wall plumes, which is given by the slope of the two curves in Fig. 3 (right panel). The ratio of these two slopes,

$$\left(1 + \frac{5C_d}{2\pi\alpha_w}\right)\frac{\alpha_w}{\alpha} = 15.2/9.6\,,$$

gives a value of the drag coefficient of $C_d \approx 0.065$, which is an order of magnitude larger than that for a boundary layer flow over a flat plate at a similar Reynolds number.

The most striking result of the simulations, which was not expected given the complex dynamics of the wall plume, is the similarity of the volume fluxes for a wall plume and one-half of a conical plume (Fig. 2, left). In light of the latest works on jet and plume turbulence

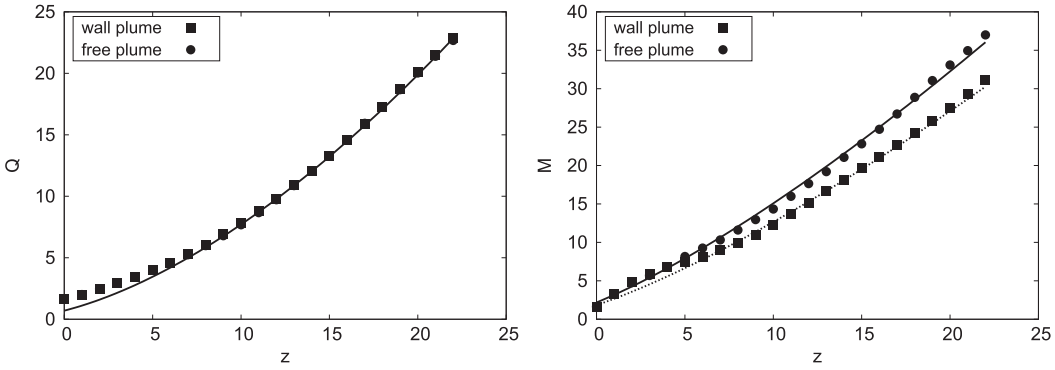

FIG. 2. (left) Volume flux and (right) momentum flux vs the vertical coordinate for the half-conical free and wall plumes. The volume flux of the wall plume is almost identical to one-half that of the conical plume; hence, the two symbols lie on top of each other and the circles in the left panel are underneath the squares. Solid curves indicate the asymptotic scaling following from the classical MTT theory and are valid for the conical plume; dashed curves indicate the asymptotic scaling following from the modified MTT theory and are valid for the wall plume (see the online supplementary material). Both theories give $Q \sim z^{5/3}$ and $M \sim z^{4/3}$. The difference is in the coefficients: $Q_w/Q = (\alpha_w/\alpha)^{4/3}(1 + 5C_d/2\pi\alpha_w)^{-1/3} = 0.97$ (dashed and solid curves are on top of each other in the left panel); $M_w/M = (\alpha_w/\alpha)^{2/3}(1 + 5C_d/2\pi\alpha_w)^{-2/3} = 0.82$, with C_d, α, and α_w obtained from DNS in our study.

(e.g., Burridge et al. 2016), one may speculate that the turbulent structures defining the entrainment in a wall plume remain similar to those in a conical plume, while only the shape of the plume "boundary" changes. To support this hypothesis, the maximum velocities in the free and wall plumes are similar, and the geometric scales of the fluctuations of the plume boundaries are similar (Fig. 4). However, the wall acts to reduce the average velocity in the wall plume as compared to the conical plume (Fig. 2), and, given the similarity of volume fluxes, the equivalent plume radius at any given height must be larger for a wall plume (Fig. 3, left panel). Given $b = (6/5)\alpha z$, the latter produces an increase in entrainment coefficient for a wall plume.

b. *Estimates of the drag coefficient for a wall plume using the measured velocity profiles*

To support the finding that the drag coefficient for a wall plume is an order of magnitude larger than that for a boundary layer flow over a flat plate, we estimated the drag coefficient from the mean velocity profiles at two different z cross sections: $z = 15$ and $z = 18$.

We fitted the velocity profiles in the vicinity of the wall with a linear function to get the slope defining the turbulent stresses (or friction velocity). The fitting function

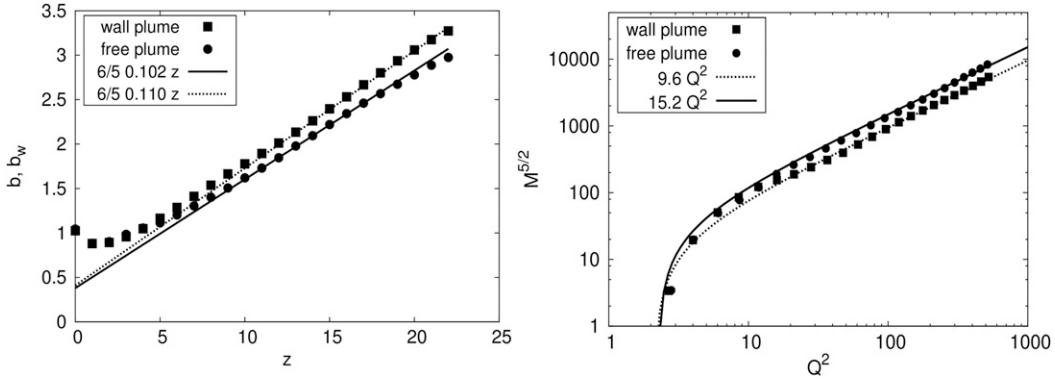

FIG. 3. (left) Free and wall plume radii (equivalent plume radius for the wall plume). Lines indicate the radius solution $b = (6/5)\alpha z$ for two different values of the entrainment coefficient; (right) $M^{5/2}$ vs Q^2 for the free and wall plumes.

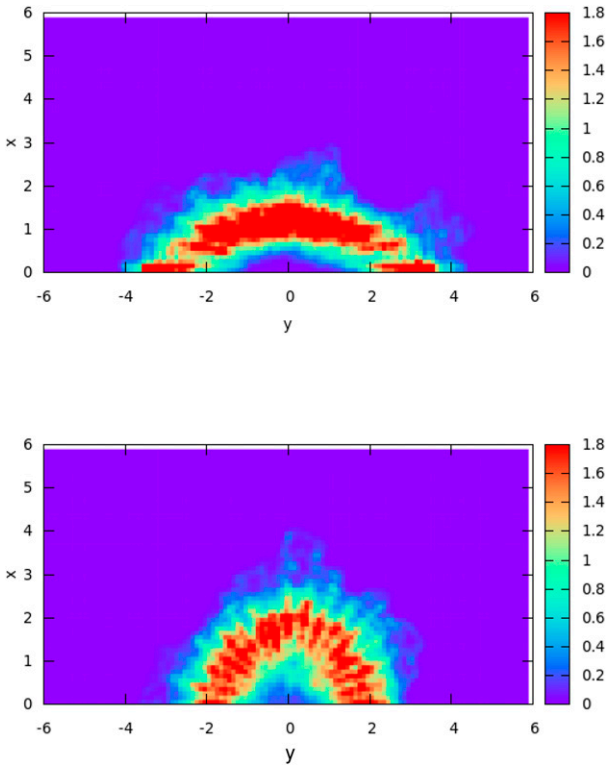

FIG. 4. Statistics of the turbulent plume boundary location at $z = 15$: (top) wall plume and (bottom) one-half of a conical plume. The figures illustrate the frequency of finding the plume boundary at a certain location (in a square of 0.1×0.1). Given the turbulent structure of the plume, the boundary is not always a single simple closed curve, because it encompasses turbulent eddies. The plume boundary is defined by the contour of density $\rho = (\tilde{\rho} - \tilde{\rho}_{pl})/(\tilde{\rho}_{amb} - \tilde{\rho}_{pl}) = 0.97$, where $\tilde{\rho}_{pl}$ is the plume density and $\tilde{\rho}_{amb}$ is the density of the ambient fluid.

is $U = x(\mathrm{Re}_0 u_*^2)$, corresponding to the inner scaling in the viscous sublayer. Then it is straightforward to calculate the viscous scale $x_v = (\mathrm{Re}_0 u_*)^{-1}$. Figure 5 displays the velocity profiles in the inner coordinates $x_+ = x/x_v$ and $U_+ = U/u_*$ at fixed y coordinate and in the cross sections $z = 15$ and $z = 18$. Note that u_* and x_v are different for the profiles at different fixed y coordinates. We also show the $(U_+ = x_+)$ dependence, characteristic of the viscous sublayer, and the classical log-law dependence $[U_+ = \ln(x_+)/0.41 + 5]$.

As can be seen, all of the velocity profiles follow the dependence typical of a viscous sublayer up to $x_+ \approx 5$, in agreement with other studies on turbulent boundary layers (e.g., Monin et al. 1971). However, farther from the wall all of the velocity profiles are lower than the classical log-law dependence. Note that even for the simpler case of a plane wall jet there is a discrepancy in log-law constants in different studies (e.g., Banyassady and Piomelli 2015); not all studies report the classical values for the parameters of $\kappa = 0.41$ and $B = 5$. We are not aware of any studies comparing the log-law dependence with the velocity profiles in 3D plumes or jets. However, the boundary layer structure of a 3D plume is more complicated when compared to that of a 2D flow. The maximum of the wall-parallel velocity in each cross section $y = \text{const}$ moves farther away from the wall as the flow propagates in the z direction and also moves farther away from the wall in each cross section $z = \text{const}$ as the plume spreads horizontally, at $|y| > 0$. Similar behavior is reported by Namgyal and Hall (2016) for a 3D wall jet. This can be considered as a smooth detachment of the flow from the wall and, in analogy with the separating (Falkner–Skan) boundary layer, might be the reason for the lower mean wall-parallel velocity in the log-law zone as compared with the classical boundary layer flow.

Table 1 summarizes the drag coefficients on the basis of the maximum vertical velocity for each profile: $C_{dm} = (u_*/U_{\max})^2 = 0.008$–$0.024$. Further, we estimate the drag coefficients, given by $C_d = (u_*/u)^2$, for all of the profiles on the basis of the cross-sectional average vertical velocity, as used in the modified MTT theory. The cross-sectional average vertical velocity, defined as $u = M/Q$, yields $u_{15} = 1.45$ and $u_{18} = 1.39$ in the cross sections at $z = 15$ and $z = 18$, respectively. The drag coefficient C_d can be estimated from the friction velocity as $\int u_*^2\, dy = 2C_d b u^2$. Introducing the local drag coefficient for each cross section, given by $C_{d,\mathrm{loc}}(y) = [u_*(y)/u]^2$, one can obtain $\int C_{d,\mathrm{loc}}(y)\, dy = 2C_d b$. We have values of $C_{d,\mathrm{loc}}(y)$ in seven y cross sections [the drag coefficient is calculated at $y = 0$, 1, 2, and 3, and, because of symmetry, $C_{d,\mathrm{loc}}(-y) = C_{d,\mathrm{loc}}(y)$]. Therefore, with the distance $\Delta y = 1$ between the different cross sections, one can get an estimate for the integral:

$$\int C_{d,\mathrm{loc}}(y)\, dy \approx \sum C_{d,i} \Delta y = (7\Delta y)\left(\sum C_{d,i}/7\right) = C_{d,\mathrm{avg}} 2B,$$

where $2B = 7\Delta y$ and $C_{d,\mathrm{avg}}$ is the average value of the local drag coefficient (see Table 1 for $C_{d,i}$). Thus, $C_d = C_{d,\mathrm{avg}}(B/b) \approx 0.04$ both for $z = 15$ and $z = 18$, which is lower but still of the same order as the results obtained in section 3a using the modified MTT equations. It is important to note that the value of the drag coefficient depends on the choice of the reference velocity U_{ref}, as follows from its definition [i.e., Eq. (1)]. Using the maximum and average vertical velocity as the reference velocity in the calculation above leads to differences in the drag coefficient of a factor of 3, a significant difference comparable to that obtained when changing the Reynolds number by three–four orders of magnitude. Hence, the choice of the drag coefficient should be consistent with the choice of the reference velocity

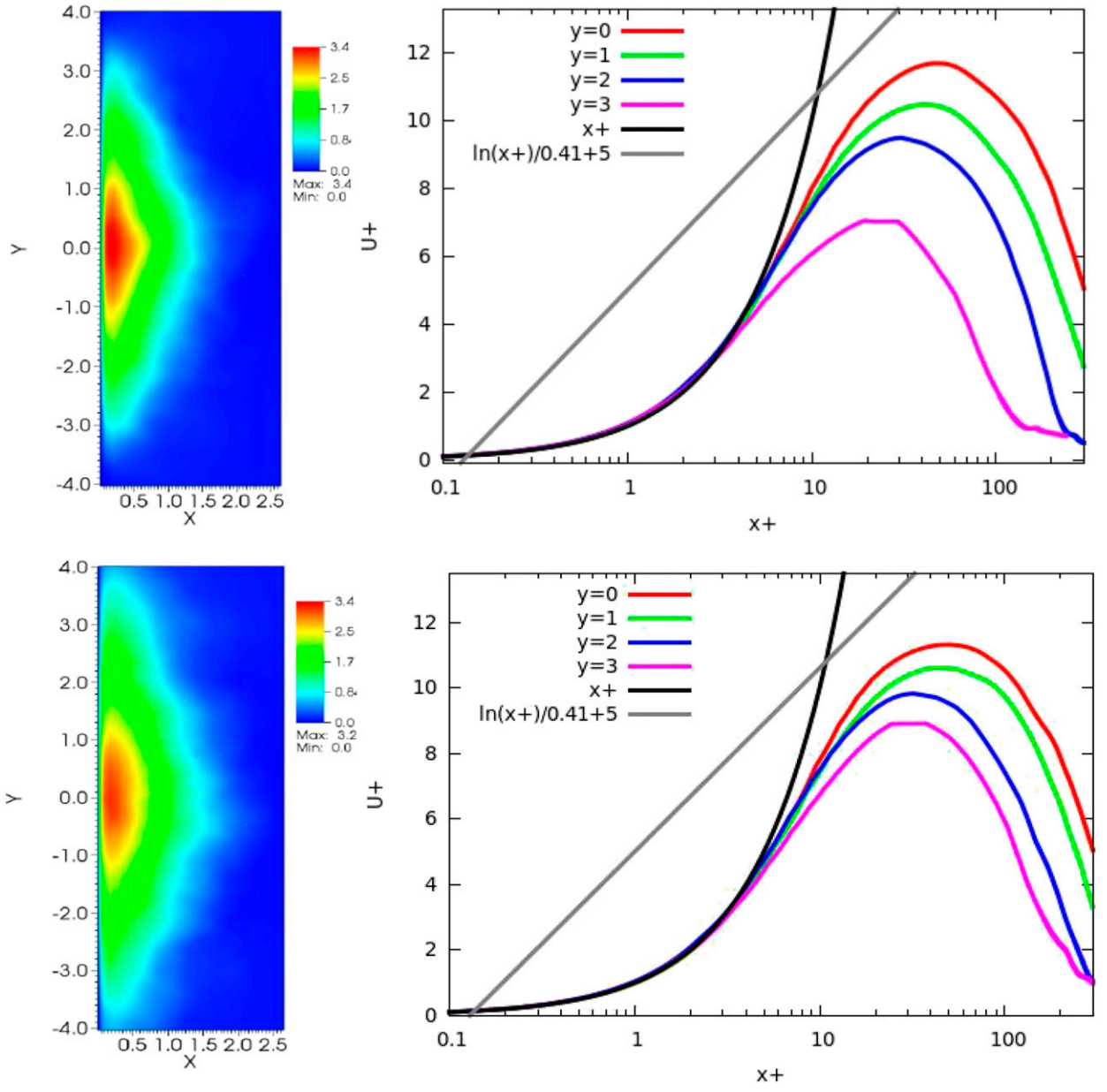

FIG. 5. (left) Horizontal cross sections and (right) profiles of the mean velocity parallel to the wall $U = (\langle u \rangle^2 + \langle v \rangle^2)^{1/2}$ in the inner coordinates at different y locations for (top) $z = 15$ and (bottom) $z = 18$.

when employing the MTT equations to obtain the subglacial discharge plume vertical velocity used in the melt parameterization.

c. *Estimates of the drag coefficient for a wall jet*

In this section, we estimate the drag coefficient using the experimental data obtained for a three-dimensional wall jet by Namgyal and Hall (2016). The drag is defined by the turbulent shear stresses, which have been observed to be similar for conical jets and plumes (van Reeuwijk et al. 2016); therefore, one could expect similar results for wall jets and plumes. These estimates can be used to test the sensitivity of the results to the Reynolds number, which in the experiment is Re = 250 000, that is, two orders of magnitude larger than in the DNS discussed in this section.

The solution of Eq. (9) for a turbulent jet is

$$M = M_0 (Q_0/Q)^{\frac{2C_d}{\pi \alpha_{\mathrm{wj}}}}, \tag{13}$$

TABLE 1. Parameters of the logarithmic near-wall flow for two z cross sections.

Parameter	$y = 0$	$y = 1$	$y = 2$	$y = 3$
$z = 15$				
u_*	0.30	0.26	0.19	0.13
x_v	0.0033	0.004	0.005	0.008
$U_{\max}$	3.38	2.72	1.80	0.84
C_{dm}	0.008	0.009	0.011	0.024
$C_{d,i}$	0.043	0.033	0.018	0.008
$z = 18$				
u_*	0.28	0.25	0.20	0.15
x_v	0.0036	0.004	0.005	0.0065
$U_{\max}$	3.10	2.59	1.90	1.27
C_{dm}	0.008	0.009	0.011	0.015
$C_{d,i}$	0.041	0.033	0.021	0.012

where $\alpha_{\rm wj}$ is the wall jet entrainment coefficient. The above expression gives the momentum flux evolution with distance from the source:

$$M = M_0\left[\sqrt{2\pi}\alpha_{\rm wj}\left(1+\frac{C_d}{\pi\alpha_{\rm wj}}\right)M_0^{1/2}Q_0^{-1}z\right]^{-\frac{2C_d}{\pi\alpha_{\rm wj}}\frac{1}{\left(1+\frac{C_d}{\pi\alpha_{\rm wj}}\right)}}. \tag{14}$$

Opposite to the wall plume results, the evolution of the wall jet "equivalent" radius involves a dependence on the drag coefficient:

$$b_{\rm wj} = \sqrt{\frac{2Q^2}{\pi M}} = 2\alpha_{\rm wj}\left(1+\frac{C_d}{\pi\alpha_{\rm wj}}\right)z.$$

The equivalent radius and momentum flux of the wall jet from the experiment of Namgyal and Hall (2016) are shown in Fig. 6. A best fit of the data in the far field allows us to determine the entrainment coefficient $\alpha_{\rm wj} \approx 0.052$, which is lower when compared with the typical entrainment coefficient for a round jet found in the literature of $0.065 < \alpha_j < 0.082$ (e.g., Fischer et al. 1979), and the drag coefficient $C_d \approx 0.032$, larger than for a flat-plate boundary layer. The difference in C_d for the wall plume ($C_d = 0.065$) and jet ($C_d = 0.032$) can be related to the difference in Reynolds number between the simulations (Re = 1000–2000) and the experiments (Re = 250 000) and probably to near-wall buoyancy effects, absent in the case of wall jets.

d. *Implications of the results for the estimates of submarine glacier melt rates*

The drag coefficient obtained in our study is 6.5 times the value used by Slater et al. (2016) ($C_d = 0.01$), is much higher than that used by Cowton et al. (2015) ($C_d = 0.0025$), and is in general an order of magnitude larger than that for a boundary layer flow over a flat plate. A large drag coefficient is expected given the relatively low Reynolds numbers; however, the difference is too large to be explained exclusively by the effect of the Reynolds number. The well-known von Kármán law for the boundary layer flow over a flat plate is

$$\frac{1}{\sqrt{c_f}} = \frac{1}{\kappa\sqrt{2}}[\ln({\rm Re}_z\sqrt{c_f}) + B_5],$$

where $B_5 = 1.7$, ${\rm Re}_z = Uz/\nu$, and $c_f = 2C_d$ (Monin et al. 1971). If, for example, we take the cross section at $z = 15$ in the region with developed turbulence, the mean vertical plume velocity increases by a factor of 1.5 from its initial value, and we obtain ${\rm Re}_z \approx 20\,000$. For this Reynolds number the drag coefficient obtained from the above von Kármán law for a flat plate is approximately $C_d = 0.005$, an order of magnitude lower than what we obtain in the simulations. Hence, the simulation results and the reasoning above suggest that also for larger Re we should expect an increased drag coefficient for a wall

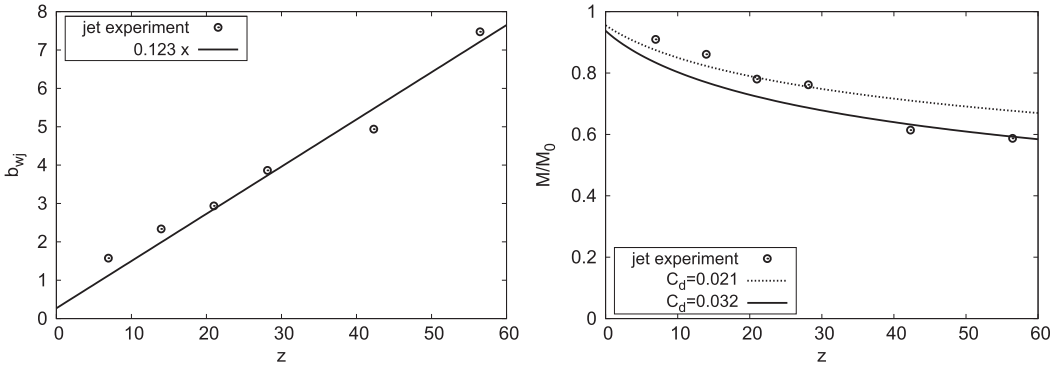

FIG. 6. (left) Equivalent wall jet radius vs vertical coordinate. (right) Momentum flux vs vertical coordinate. Dashed and solid curves represent approximations to near-field and far-field data, respectively. The data are taken from the wall jet experiment by Namgyal and Hall (2016).

plume. This increase in C_d is a critical factor in the current parameterization for submarine melting.

The present study suggests that $C_d = 0.001$ is an inappropriate estimate of the drag coefficient when using the modified MTT model with a top hat velocity profile. The drag decrease with increasing Reynolds number can be expected to be similar to that following from the von Kármán law and reliably quantified for the boundary layer flow over a flat plate (e.g., Monin et al. 1971). The von Kármán law suggests a decrease by a factor of 4–5 of the drag coefficient from the low ($\mathrm{Re} \approx 10^4$) to high ($\mathrm{Re} \approx 10^9$) Reynolds numbers; thus, the value of $C_d = 0.065$ obtained for $\mathrm{Re}_z = 20\,000$ corresponds to a value $C_d = 0.01$–0.02 for the large Reynolds numbers, relevant to geophysical flows. This is in agreement with the value 0.01 used by Slater et al. (2016). Note that the lower value of the drag coefficient due to a larger Re obtained for a wall jet in section 3c is also consistent with that predicted by the von Kármán law. In addition, given that some important phenomena, such as sediment load within the subglacial discharge plumes and glacier surface roughness, are not considered in our study, the drag coefficient relevant to geophysical flows is likely larger than 0.01–0.02.

We finally discuss the implications of the larger value of the drag coefficient obtained using the modified MTT theory, which is often implemented to calculate the subglacial discharge plume velocity used in the melt-rate parameterizations. From the three-equation melt formulation (Holland and Jenkins 1999), the melt rate is proportional to the friction velocity or, using Eq. (1), to the mean vertical plume velocity: $\dot{m} \approx uC_d^{1/2}$, where $C_d = 0.01$ is used by Slater et al. (2016) [0.0025 by Cowton et al. (2015)] and u can be obtained from MTT theory neglecting the wall effects. Within the same framework, improved with Eq. (12) to account for the presence of the wall, the melting rate can be written as

$$\dot{m}_w \approx u\left(\frac{\alpha}{\alpha_w}\right)^{2/3} \frac{C_d^{1/2}}{\left(1+\dfrac{5C_d}{2\pi\alpha_w}\right)^{1/3}},$$

with the velocity u from MTT theory without a wall. This dependence of the melt rate on the drag coefficient is illustrated in Fig. 7, with the melt rate normalized by that obtained with the frequently used drag coefficient $C_d = 0.0025$. Thus, the estimate of melt rate for $C_d = 0.01$–0.02 is more than 2 times that obtained using $C_d = 0.0025$. Moreover, from van Kessel and Kranenburg (1996), it follows that up to a factor-of-3 increase in the drag coefficient can be expected when sediments are present in the flow. Thus the melt rate can grow further to yield as much as ~4–5 times that for $C_d = 0.0025$ if the sediment load and a roughness of the glacier surface are taken into account. Given the nonnegligible change in melt rates, additional investigations are therefore needed to characterize the dependence of C_d on Reynolds numbers and its sensitivity to the sediment load.

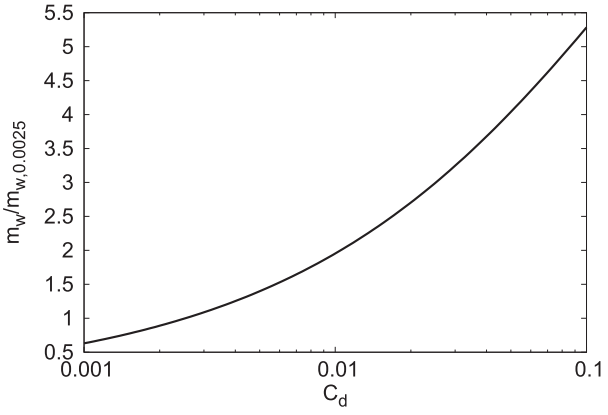

FIG. 7. Melt-rate dependence on the drag coefficient. The melt rate is normalized by that obtained using $C_d = 0.0025$.

4. Conclusions

We have shown that classical plume theory can form the basis of improved models of three-dimensional wall plumes if the wall drag is accounted for and the entrainment coefficient is corrected. The volume flux evolution of a wall plume is well captured already by considering one-half of that obtained for a conical plume, which implies that the dilution of the wall plume fluid, that is, the salinity and temperature evolution with depth, should also be predicted reasonably well when neglecting drag effects. The difference is only in the momentum flux, which is overestimated by about 10%–20% if the wall drag is not accounted for. However, the coefficients parameterizing turbulence effects for entrainment, drag, and scalar transfer are important for the predictions of melting rates, because these coefficients appear in the widely used three-equation melt formulation (Holland and Jenkins 1999). We have shown that a consistent estimate of the drag coefficient that is based on the modified MTT theory plume velocity and a corrected vertical velocity for wall plumes that takes into account a nonnegligible drag coefficient [Eq. (12)], substantially increase the predictions for melting rates near an ice wall. Furthermore, we have shown for the first time that the wall plume spreads horizontally parallel to the wall and loses its axisymmetric shape (Fig. 1, top- and bottom-right panels). This important aspect will produce an increase in melting when compared with that obtained with a half-conical plume because of the larger area covered on an ice face by the wall plume.

Adding the mass and buoyancy fluxes associated with melting into the wall plume model is not expected to alter our results significantly. In general, a subglacial discharge is characterized by a volume flux $Q \approx 100\,\mathrm{m^3\,s^{-1}}$, corresponding to a "convection-driven melting" regime (Jenkins 2011), in which the contribution of submarine melting to the plume buoyancy is small. It is only for a small discharge, $\sim 10\,\mathrm{m^3\,s^{-1}}$ (Mankoff et al. 2016; Ezhova et al. 2017), that the effect of submarine melting on the plume buoyancy flux cannot be neglected. Both drag and entrainment are mainly influenced by the turbulent characteristics of the wall plume, which, for substantial subglacial discharges, should remain unchanged.

Our study shows that the increase in C_d for a modified MTT model of a three-dimensional wall plume at large Reynolds numbers can be as high as 10 times as compared with that associated with a 2D turbulent boundary layer flow ($C_d = 0.001$) and, thus, cannot be ignored while calculating melting rates.

Acknowledgments. This work was supported by the Linné FLOW Centre at KTH and the Academy of Finland Center of Excellence Programme Grant 307331 (author Ezhova) and by VR Swedish Research Council Grant VR 2014-5001 (author Brandt). Support to author Cenedese was given by NSF Project OCE-1434041. Computer time was provided by the Swedish National Infrastructure for Computing (SNIC). Visualization and graphic analysis were performed with VisIt (Childs et al. 2012) and Gnuplot.

REFERENCES

Banyassady, R., and U. Piomelli, 2015: Interaction of inner and outer layers in plane and radial wall jets. *J. Turbul.*, **16**, 460–483, https://doi.org/10.1080/14685248.2015.1008008.

Burridge, H. C., G. R. Partridge, and P. F. Linden, 2016: The fluxes and behaviour of plumes inferred from measurements of coherent structures within images of the bulk flow. *Atmos.–Ocean*, **54**, 403–417, https://doi.org/10.1080/07055900.2016.1175337.

Childs, H., and Coauthors, 2012: VisIt: An end-user tool for visualizing and analyzing very large data. *High Performance Visualization–Enabling Extreme-Scale Scientific Insight*, W. Bethel, C. Hank, and H. Charles, Eds., Taylor and Francis, 357–372.

Cowton, T., D. Slater, A. Sole, D. Goldberg, and P. Nienow, 2015: Modeling the impact of glacial runoff on fjord circulation and submarine melt rate using a new subgrid-scale parameterization for glacial plumes. *J. Geophys. Res. Oceans*, **120**, 796–812, https://doi.org/10.1002/2014JC010324.

Craft, T. J., and B. E. Launder, 2001: On the spreading mechanism of the three-dimensional turbulent wall jet. *J. Fluid Mech.*, **435**, 305–326, https://doi.org/10.1017/S0022112001003846.

Ezhova, E., C. Cenedese, and L. Brandt, 2017: Dynamics of a turbulent buoyant plume in a stratified fluid: An idealized model of subglacial discharge in Greenland Fjords. *J. Phys. Oceanogr.*, **47**, 2611–2630, https://doi.org/10.1175/JPO-D-16-0259.1.

Fischer, H. B., E. List, R. Koh, J. Imberger, and N. Brooks, 1979: *Mixing in Inland and Coastal Waters.* Academic Press, 302 pp.

Gayen, B., R. W. Griffiths, and R. C. Kerr, 2016: Simulation of convection at a vertical ice face dissolving into saline water. *J. Fluid Mech.*, **798**, 284–298, https://doi.org/10.1017/jfm.2016.315.

Holland, D. M., and A. Jenkins, 1999: Modelling thermodynamic ice–ocean interactions at the base of an ice shelf. *J. Phys. Oceanogr.*, **29**, 1787–1800, https://doi.org/10.1175/1520-0485(1999)029<1787:MTIOIA>2.0.CO;2.

Jenkins, A., 2011: Convection-driven melting near the grounding lines of ice shelves and tidewater glaciers. *J. Phys. Oceanogr.*, **41**, 2279–2294, https://doi.org/10.1175/JPO-D-11-03.1.

——, K. W. Nicholls, and H. F. Corr, 2010: Observation and parameterization of ablation at the base of Ronne ice shelf, Antarctica. *J. Phys. Oceanogr.*, **40**, 2298–2312, https://doi.org/10.1175/2010JPO4317.1.

Launder, B. E., and W. Rodi, 1983: The turbulent wall jet—Measurements and modelling. *Annu. Rev. Fluid Mech.*, **15**, 429–459, https://doi.org/10.1146/annurev.fl.15.010183.002241.

Mankoff, K. D., F. Straneo, C. Cenedese, S. B. Das, C. D. Richards, and H. Singh, 2016: Structure and dynamics of a subglacial discharge plume in a Greenland Fjord. *J. Geophys. Res. Oceans*, **121**, 8670–8688, https://doi.org/10.1002/2016JC011764.

Monin, A. S., A. M. Yaglom, and J. L. Lumley, 1971: *Statistical Fluid Mechanics: Mechanics of Turbulence*. Vol. 1. 1st ed. MIT Press, 782 pp.

Morton, B. R., G. Taylor, and J. S. Turner, 1956: Turbulent gravitational convection from maintained and instantaneous sources. *Proc. Roy. Soc. London*, **234A**, 1–25, https://doi.org/10.1098/rspa.1956.0011.

Namgyal, L., and J. W. Hall, 2016: Reynolds stress distribution and turbulence generated secondary flow in the turbulent three-dimensional wall jet. *J. Fluid Mech.*, **800**, 613–644, https://doi.org/10.1017/jfm.2016.404.

Slater, D. A., D. N. Goldberg, P. W. Nienow, and T. R. Cowton, 2016: Scalings for submarine melting at tidewater glaciers from buoyant plume theory. *J. Phys. Oceanogr.*, **46**, 1839–1855, https://doi.org/10.1175/JPO-D-15-0132.1.

Straneo, F., and C. Cenedese, 2015: Dynamics of Greenland's glacial fjords and their role in climate. *Annu. Rev. Mar. Sci.*, **7**, 89–112, https://doi.org/10.1146/annurev-marine-010213-135133.

van Kessel, T., and C. Kranenburg, 1996: Gravity current of fluid mud on sloping bed. *J. Hydraul. Eng.*, **122**, 710–717, https://doi.org/10.1061/(ASCE)0733-9429(1996)122:12(710).

van Reeuwijk, M., P. Salizzoni, G. R. Hunt, and J. Craske, 2016: Turbulent transport and entrainment in jets and plumes: A DNS study. *Phys. Rev. Fluids*, **1**, 074301, https://doi.org/10.1103/PhysRevFluids.1.074301.